Paper ID: CE 0263

Effectiveness of ECC Encasement on the Compressive Behavior of Slender CFST Column- A Numerical Study

N. Ahmed[1], M. S. Hossain[2], M. H. Hridoy[3], M. I. Kabir[4]

[1]Department of Civil & Environmental Engineering, IUT, Bangladesh (nazibahmed@iut-dhaka.edu)
[2]Department of Civil & Environmental Engineering, IUT, Bangladesh (shahriarrif@gmail.com)
[3]Department of Civil & Environmental Engineering, IUT, Bangladesh (mehedihassan45@iut-dhaka.edu)
[4]Department of Civil & Environmental Engineering, IUT, Bangladesh (imran.kabir@iut-dhaka.edu)

Abstract

This paper presents a numerical investigation on the compressive behavior of Engineered Cementitious Composite (ECC) encased slender Concrete Filled Steel Tube (CFST) columns under concentric loading. Using ABAQUS, a detailed Finite Element (FE) model was created to investigate the columns' compressive behavior. The FE model was first validated against the existing test results and then employed to conduct a comprehensive parametric study. In the parametric study, the impacts of different parameters, for example, the concrete-to-steel ratio, the thickness of the ECC layer, the strength of the steel tube, the compressive strength of the ECC and the core concrete was studied on the compressive behavior of the columns. The parametric study provided valuable insights into the compressive behavior of slender ECC-CFST columns under concentric loading and highlighted the potential application of ECC as effective encasing material for enhancing the performance of CFST columns. Furthermore, this study investigated the modes of failure of the columns, including buckling of the local steel tube and the crushing of the concrete. The results of this study showed that ECC, as an encasing material significantly improved the load-carrying capacity of columns under compression. The findings of this study would be beneficial for day-to-day design practitioners.

Keywords: *Finite element analysis; engineered cementitious composites; ECC encasement; concrete-filled steel tube; compressive behavior.*

1 Introduction

Composite structures have widely been applied in modern constructions, where both steel and concrete materials are combined to form a structure that is stronger and more durable than the structure made up by either material. One of the most common forms of composite columns is Concrete Filled Steel Tube (CFST) column which recently has gained huge popularity. When compared to conventional reinforced concrete columns, this form of composite column reduces the self-weight of the member significantly while maintaining high strength and stiffness. However, under high amount of compressive loading, CFST column with slender steel tube might buckle before the full plastic moment is achieved. Thus, attention must be paid to ensure structural stability. Towards this end, Engineered Cementitious Composites (ECC)-a high-performance fiber-reinforced cementitious composite, can be applied to encase the CFST column to improve the compressive behavior of slender CFST columns due to its excellent ductility.

Various studies related to concrete encased CFST columns under different loading conditions were conducted extensively. Zhang et al.'s (2020) work provided a comprehensive overview of the behavior of concrete encased CFST columns by highlighting the factors that influence their performances. The study emphasized the use of theoretical models to predict the strength and stiffness of concrete encased CFST columns. Although the prescribed models showed excellent performance in predicting strength and stiffness, yet they failed in predicting column ductility. Cai et al. (2020) presented the behavior of eccentrically loaded CFST columns encased with ECC. Their research employed a combination of experimental testing and numerical modeling to investigate the response of ECC-encased CFST columns under eccentric loading. The findings contributed greatly to the design and construction of ECC-encased CFST columns, enhancing their load-carrying capacity and ductility. This research further suggested that ECC-encased CFST columns exhibited superior load-carrying capacity and ductility compared to conventional CFST columns when subjected to eccentric loading conditions.

However, this study was only focused on the CFST columns with compact steel tube section. Zhang et al. (2021) investigated the feasibility of strengthening slender CFST columns through textile-reinforced engineered cementitious composites (TR-ECCs). The study results showed that TR-ECC enhanced the load-carrying capacity, stiffness, and ductility of slender CFST columns under axial compression. By going through a meticulous literature review and evaluation of prior research, this study aimed to investigate the effectiveness of ECC encasement on the compressive behavior of slender CFST column under pure compressive loading. Hence, a detailed Finite Element (FE) model was created to investigate the proposed columns' compressive behavior under pure compressive loading. The FE model was first validated against the existing test results and then employed to conduct a comprehensive parametric study. The results obtained from this study would contribute to the existing knowledge and pave the way for future research endeavors.

2 Development of the Finite Element (FE) Model

Finite Element (FE) analysis was used to analyze the structural behavior of an ECC-encased CFST column by evaluating load-carrying capacity, stress distribution, and deformation characteristics. The FE models of the studied columns were developed in ABAQUS. The following sections discuss the development of the FE model.

2.1 Constitutive material model for core concrete, steel and ECC

The steel tube encased the core concrete exhibits higher ductility than regular concrete (Cai et al., 2017). Core concrete's key mechanical properties including the compressive strength (35 MPa) and elastic modulus (33000 MPa) were considered in the FE model. The concrete damage plasticity (CDP) model was employed for defining the plastic properties of core concrete. The material properties of the core concrete were defined using the following constitutive equations from Cai et al. (2020).

$$\varepsilon_{co} = 0.00076 + \sqrt{(0.626f'_c - 4.33)} \times 10^{-7} \quad (1)$$

Since the effect is minimal in the initial stage, the constitutive model for core concrete is the same as that for normal concrete. In the last stage the model can be defined by:

$$\sigma = 0.1f'_c + 0.9f'_c exp\left[-\left(\frac{\varepsilon-\varepsilon_c}{\alpha}\right)^{0.92}\right] \qquad \varepsilon \geq \varepsilon_c \quad (2)$$

$$\alpha = 0.005 + .0075\xi_c \quad (3)$$

$$\xi_c = \frac{A_S f_y}{A_c f_{ck}} \quad (4)$$

Where, f'_c and f_{ck} are the cylinder strength and characteristic strength of concrete, A_s and A_c are the cross sectional areas of steel tube and concrete, ε is the yield strain of concrete, ε_c is the first cracking strain of concrete.

For the steel tube and reinforcing rebars, treated as isotropic elastic-plastic, were modeled in the FE models using properties like elastic modulus (200000 MPa) portraying stiffness, and Poisson's ratio (0.3) indicating how axial loads alter material dimensions. These parameters capture stress-strain relationships and lateral-to-axial strain behavior. Han et al.'s (2007) stress-strain model was used as the constitutive model for steel tubes and steel reinforcements, as shown below:

$$\sigma_s = \begin{cases} f_y & \varepsilon_e < \varepsilon_s < \varepsilon_{e1} \\ \left[1 + 0.6\frac{\varepsilon_s-\varepsilon_{e1}}{\varepsilon_{e2}-\varepsilon_{e1}}\right] f_y & \varepsilon_{e1} < \varepsilon_s < \varepsilon_{e2} \\ 1.6f_y & \varepsilon_s > \varepsilon_{e2} \end{cases} \quad (5)$$

Where, $\varepsilon_e = \frac{0.8f_y}{E_S}$, $\varepsilon_{e1} = 1.5\varepsilon_e$, $\varepsilon_{e2} = 10\varepsilon_e$, f_y is the yield strength of steel, E_s is the elastic modulus and ε_s refers to the yield strain of steel.

For the compressive behavior of ECC, similar to the core concrete, CDP model was used to define it's elastic and plastic properties. Experimentally obtained compressive strength of 30 MPa, with elastic modulus of 15500 MPa, and Poisson's ratio of 0.2 is used. The tensile behavior of ECC was simulated using the reduced bilinear curves, which is proposed by Tao et al. (2013) and Li et al. (2017) shown below:

$$\varepsilon_o = \varepsilon_{co} + 800\xi^{0.2} \times 10^{-6} \quad (6)$$

$$\varepsilon_{co} = (1300 + 12.5f_{co}) \times 10^{-6} \quad (7)$$

$$\frac{\sigma_c}{f_{co}} = \{2\left(\frac{\varepsilon_c}{\varepsilon_o - \left(\frac{\varepsilon_c}{\varepsilon_o}\right)^2}\right)_{(\varepsilon_c \leq \varepsilon_o)} \frac{\left(\frac{\varepsilon_c}{\varepsilon_{co}}\right)}{\beta_o\left[\left(\frac{\varepsilon_c}{\varepsilon_o}\right)-1\right]^2+\left(\frac{\varepsilon_c}{\varepsilon_o}\right)} \qquad \varepsilon_c > \varepsilon_o \quad (8)$$

$$\beta_o = (2.36 \times 10^{-5})^{[0.25+(\xi-0.5)^7]}(f_{co})^{0.5} \times 0.5 \geq 0.12 \quad (9)$$

Where, f'_{co} is the compressive strength of concrete, σ_c is the cracking strength of ECC, β_o is the stirrup confinement index for ECC, ξ is shape factor, ε_{co} is the yield strain of ECC, ε_c refers to peak strain of ECC, ε_o is the first cracking strain of ECC.

2.2 Selection of elements, applied constraint, load and boundary conditions

For the selection of the elements, while solid elements with reduced integration (C3D8R) were selected for steel tube, core concrete and ECC parts, truss elements (T3D2) were chosen for the reinforcing bars. In addition, two rigid plates (placed at top and bottom of the column) were modeled using the rigid body elements (R3D4). These two plates were tied at top and bottom of the column using the "TIE CONSTRAINT" feature of ABAQUS to ensure a solid connection between the plates and the composite column. The interaction between the core concrete to steel tube and ECC to steel tube was developed by describing the normal and tangential contact behavior using hard contact and Mohr-Coulomb friction models. Friction co-efficient of 0.25 and 0.4 were chosen to define the interaction between concrete to steel tube and ECC to steel tube. As the bond-slip behavior between ECC and steel was not studied, but adhesive bond stress is significantly greater than between concrete and steel, hence, a higher friction co-efficient was chosen for defining the interaction between ECC to steel tube. Further to the material property, element selection, and definition of interaction, two reference points were created at the center of rigid plates to apply the load and boundary conditions. The displacement-controlled loading was applied at the reference point of top rigid plate by restraining all degrees of freedom except the vertical displacement. A vertical displacement of 10 mm was applied for the purpose of load application. The fixed boundary conditions were ensured at the bottom end of the column by restraining all degrees of freedom of the reference point. A total of four FE models were created for the validation purpose. The specifications of the developed FE model are listed in Table 1 and the typical model geometry proposed by Cai et al. (2018) is shown in Figure1.

Table 1. Test Specimen

Specimen	Material	Stirrup Spacing, (mm)	a_1	a_2	t (mm)
C1-ECC	ECC	100	1%	0.40%	6
C2-ECC	ECC	200	1%	0.20%	6
C3-ECC	ECC	100	1%	0.40%	10
C4-ECC	ECC	100	0.50%	0.40%	6

Note: t, a_1 and a_2 are the thickness steel tube ratio and longitudinal reinforcement ratio.

Figure 1. Typical model geometry of ECC encased CFST column

3 Validation of the Developed FE Model

The predicted load bearing capacity of the ECC-encased CFST columns by the FE model was compared with existing test results in Table 2. The results obtained from the FE simulation is slightly less than the experimental results which is possibly due to underestimated confinement impact on core concrete.

Table 2. The comparison of axial load carrying capacity

Specimens	Experimental (N_u)	Computational (N_{cu})	N_u/N_{cu}
C1-ECC	5197	4891	0.94
C2-ECC	5148	4921	0.96
C3-ECC	6257	5993	0.96
C4-ECC	5069	4783	0.94

The failure mode obtained from the FE model was also compared with the test observations in Figure 2 and 3. Again, it is observed that from the FE model can predict the failure mode of the studied columns with sufficient accuracy by showing the plastic deformation in the center of composite column.

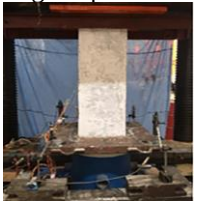

Figure 2. Test specimen from Cai et al. (2018).

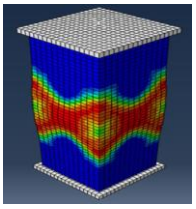

Figure 3. FE Model

4 Compressive Behavior of ECC encased CFST-Column Subjected to Concentric Loading

In the parametric study the load-carrying capacity and the failure modes of the ECC encased CFST columns were investigated for different ECC thicknesses and steel tube diameters. The specifications of the studied models are outlined in Table 3. The parameters included were cross-section ratio (D/B), longitudinal reinforcement ratio (D/t), steel tube ratio, steel tube strength, and concrete strength and ECC strength. Studying these factors would provide valuable insights for engineers to enhance the design and properties of CFST columns, ensuring strength, stiffness, and overall performance. The following sections will describe the results obtained from the parametric study.

Table 3. ECC encased CFST columns' dimensions and material properties

Parameter	Specimen	Specimen size								Material properties			
		B (mm)	D (mm)	t (mm)	D/B	D/t	A_l (mm^2)	α_t	α_l	f_{Eck} (MPa)	f'_c (MPa)	f_{Sy} (MPa)	γ
ECC strength	ES-1	300	180	1.25	0.6	144	400	0.038	0.25%	30	35	350	0.94
	ES-2	300	180	1.25	0.6	144	400	0.038	0.25%	50	35	350	0.95
	ES-3	300	180	1.25	0.6	144	400	0.038	0.25%	70	35	350	0.95
Concrete strength	CS-1	300	180	1.25	0.6	144	400	0.038	0.25%	50	30	350	0.93
	CS-2	300	180	1.25	0.6	144	400	0.038	0.25%	50	50	350	0.95
	CS-3	300	180	1.25	0.6	144	400	0.038	0.25%	50	70	350	0.95
Steel tube strength	SS-1	300	180	1.25	0.6	144	400	0.038	0.25%	50	50	350	0.96
	SS-2	300	180	1.25	0.6	144	400	0.038	0.25%	50	50	690	0.94
	SS-3	300	180	1.25	0.6	144	400	0.038	0.25%	50	50	960	0.98
Steel tube ratio	TR-1	300	180	1	0.6	180	400	0.038	0.25%	50	50	350	0.94
	TR-2	300	180	1.25	0.6	144	400	0.052	0.25%	50	50	350	0.95
	TR-3	300	180	1.5	0.6	120	400	0.066	0.25%	50	50	350	0.94

Note: f_{Eck}, f'_c and f_{Sy} are the compressive strength of ECC, concrete and steel, respectively. B is the square section's side length, D is the steel tube's outer diameter, t is the thickness of the steel tube, Al is the cross-sectional area, αt is the steel tube ratio, αl is the longitudinal reinforcement ratio and γ is the combination coefficient of ECC-encased CFST column.

4.1 Effects of ECC Strength

Figure 4(a) illustrates the load-displacement graph for varying strengths of ECC. The load-displacement graph highlights that ES-03 exhibited a greater load-bearing capacity compared to ES-02 and ES-01, attributed to its higher compressive strength. The graph indicates that the maximum load-bearing capacities are 3306.68 kN for ES-02, 4528.39 kN for ES-01, and 5839.86 kN for ES-03. A comparison between ECC encased CFST columns and conventional CFST and bare steel tube columns demonstrates that ECC encased CFST columns possess a superior load-carrying capacity in contrast to conventional CFST and steel tubes.

4.2 Effects of Concrete Strength

The load-displacement graph as shown in Figure 4 (b) for the different concrete strength specimens reveals that CS-03 exhibited a higher load-bearing capability in comparison to CS-02 and CS-01, owing to its higher compressive strength. As discerned from the graph, the maximum load capacity is 4416.09 kN for CS-01, which increases to 4863.93 kN for CS-02, and further rises to 5118.48 kN for CS-03.

4.3 Effects of Steel Tube Strength

The load-displacement graph presents various specimens with distinct steel tube strengths in Figure 4(c). It is observed that SS-03 can withstand a greater load compared to SS-02 and SS-01 as the yield strength of steel tube rises from 350 MPa to 950 MPa. As indicated in the graph, the maximum load capacity was 4863.51 kN for SS-01, which increased to 5447.03 kN for SS-02, and further rose to 5537.57 kN for SS-03.

4.4 Effects of Steel Tube Ratio Strength

The load-displacement graph depicting different specimens with varying steel tube ratios is presented in Figure 4(d). It shows that TR-03 can sustain a higher load in comparison to TR-02 and TR-01, due to its greater steel tube thickness. TR-03's steel tube exhibits a thickness of 1.5 mm, whereas TR-02 and TR-01 have steel tube thicknesses of 1.25 mm and 1 mm, respectively. As observed from the graph, the maximum load capacity was 4804.33 kN for TR-01, which increased to 4863.51 kN for TR-02, and further advanced to 4920.37 kN for TR-03.

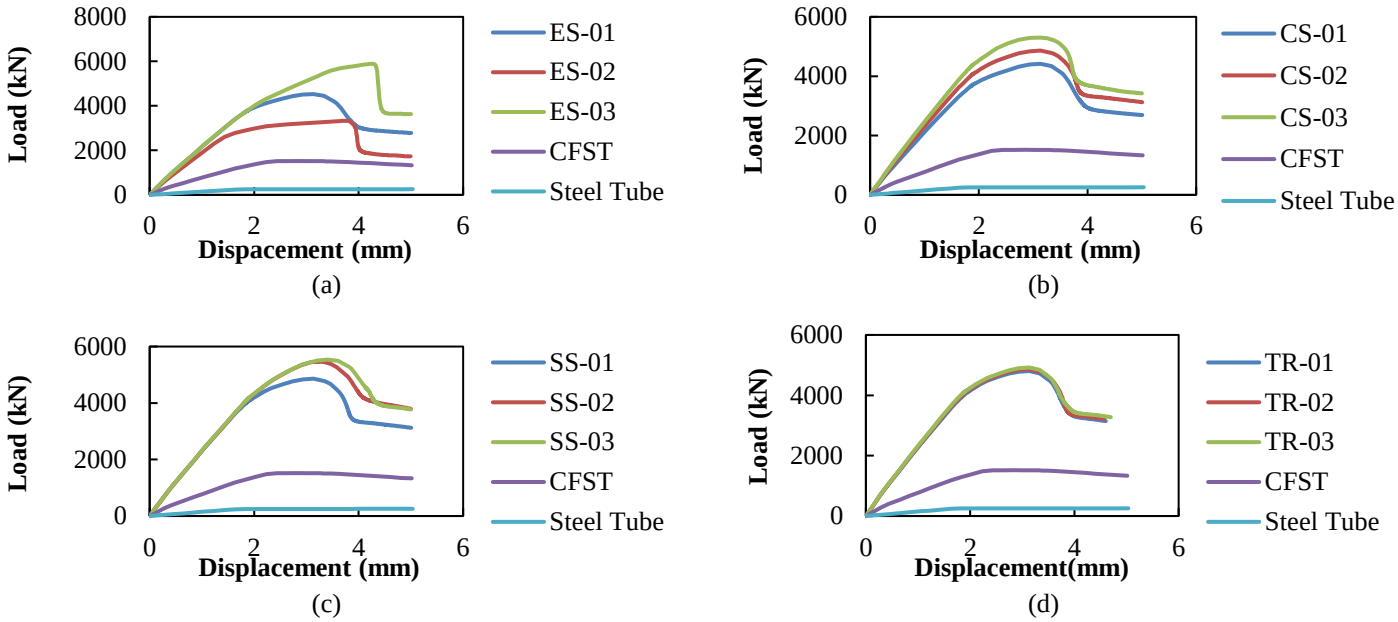

Figure 4. (a) Strength of ECC (b) Strength of Concrete (c) Strength of Steel Tube (d) Strength of Steel Tube Ratio

4.5 The Ultimate Strength of ECC-encased CFST Column

The combined behavior of steel tubes, concrete core, and ECC material were taken into consideration when determining an ECC-encased CFST column's ultimate strength. Steel tube provided structural support, while concrete core's strength and stiffness were determined by compressive strength and confinement. ECC material improved CFST column strength, ductility, and fracture resistance. Accurate numerical model representation of parameters is crucial for realistic simulation results and column performance optimization.

Table 4. The Load Carrying Capacity of FEM Models

Parameter	Specimen	Ultimate load from FEM, $P_{ECC-CFST}$, KN	Ultimate load for CFST column, P_{CFST}, KN	Ultimate load for Steel, KN	$P_{ECC-CFST}/P_{CFST}$	Load Carrying Capacity (%)
ECC strength	ES-1	4528.39	1513.09	256.25	2.99	66.58
	ES-2	3306.68			2.18	54.24
	ES-3	5839.56			3.85	74.08
Concrete strength	CS-1	4416.09			2.91	65.73
	CS-2	4863.93			3.21	68.89
	CS-3	5118.48			3.38	70.43
Steel tube strength	SS-1	4863.51			3.21	68.88
	SS-2	5447.03			3.59	72.22
	SS-3	5537.57			3.65	72.67
Steel tube ratio	TR-1	4804.33			3.17	68.50
	TR-2	4863.51			3.21	68.88
	TR-3	4920.37			3.25	69.24

4.6 Failure Modes

When loose concrete is removed, the model exhibited conventional failure modes, with local yielding seen in several areas and considerable out-of-plane local buckling of steel tube and reinforcement shown in Figure 5. The concrete strength, steel tube strength, and steel tube ratio test specimens failed as a result of concrete spalling and crushing. In ECC strength specimens shown in Figure 5(b), there is a new failure mode with three phases. Minor cracks start in the first stage, which is followed by the growth and extension of already-existing cracks. In the last phase, the outer ECC separates from the inner steel tube. This result is similar to those observations obtained by Li et al. (2020).

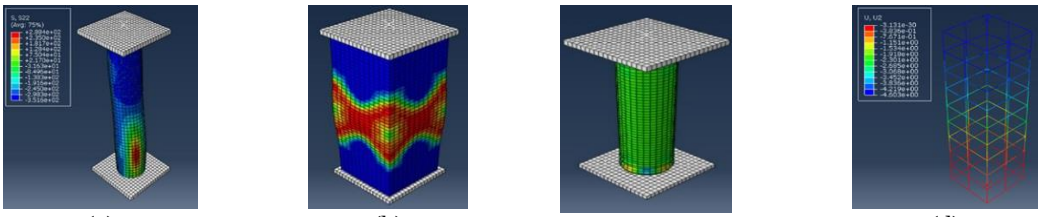

(a) (b) (c) (d)

Figure 5. Failure modes of (a) CFST Column, (b) ECC, (c) Steel tube and (d) Reinforcement

5 Conclusions

The performance of various specimens with different material properties and strengths were investigated in this study. The comparison between ECC encased specimens and conventional CFST and bare steel tube columns revealed that ECC encased specimens demonstrated a higher load-carrying capacity compared to conventional CFST and bare steel tube columns. This is because of the ECC encasement which allowed the slender steel tube to attain its full plastic capacity without showing any outward buckling. Thus, the implications of these findings would promote the application of conventional CFST column with slender steel tube by encasing it with ECC particularly for high rise construction.

References

An, Y.F., Han, L.H., and Zhao, X.L. (2007). Behavior and design calculations on very slender thin-walled CFST columns. Thin-Walled Structures, Vol. 53, No. 02, pp. 161–175.

Z. Tao, Z.B. Wang, Q. Yu (2013). Finite element modelling of concrete-filled steel stub columns under axial compression. J. Constr. Steel Res., Vol. 89, pp. 121–131.

Li, G.C., Zhou, B., and Pan, J.H. (2014). Finite Element Analysis on Concrete-Filled Square Steel Tube Short Columns with Inner CFRP Profiles under Axial Compression. Applied Mechanics and Materials, Vols. 578-579, pp. 335–339.

Han, L.H., and An, Y.F. (2014). Performance of concrete encased CFST stub columns under axial compression. Journal of Constructional Steel Research, Vol. 100, pp. 70–85.

Yu, W., and Zhang, Y. (2016). Experimental study on eccentrically loaded concrete-filled steel tubular (CFST) columns with or without ECC. Construction and Building Materials, Vol. 122, pp. 408–417.

Cai, J., Zhang, L., Tan, J., and Li, X. (2017). Experimental behavior of short circular CFST stub columns filled with engineered cementitious composites under axial compression. Journal of Constructional Steel Research, Vol. 137, pp. 99–108.

Y. Li, Z. Liu, W. Wang, et al. (2017). Experimental study on axial compression performance of ECC confined with stirrups, J. Build. Struct. Vol. 13(7), pp 1748.

Cai, J., Pan, J., and Li, X. (2018). Behavior of ECC-encased CFST columns under axial compression. Journal of Constructional Steel Research, Vol. 171, pp. 1–9.

Cai, J., Pan, J., Tan, J., Vandevyvere, B., and Li, X. (2020). Behavior of ECC-encased CFST columns under eccentric loading. Journal of Building Engineering, Vol. 30, pp. 101188.

Cai, J., Pan, J., Lu, C., and Li, X. (2020). Nonlinear analysis of circular concrete-filled steel tube columns under eccentric loading. Magazine of Concrete Research, Vol. 72, No. 6, pp. 292–303.

Zhang, L., Zhang, X., Cai, J., and Li, X. (2020). Behavior of square CFST columns with inner ECC under axial compression. Engineering Structures, Vol. 203, pp. 110058.

Huang, Y., Li, W., Lu, Y., Liang, H., and Yan, Y. (2022). Behavior of CFST slender columns strengthened with steel tube and sandwiched concrete jackets under axial loading. Engineering Structures, Vol. 45, pp. 103613.